On the PAPR Characteristics of DFT-s-OFDM with Geometric and Probabilistic Constellation Shaping

Anastasios Kakkavas*†, Wen Xu*, Jian Luo*, Mario Castañeda* and Josef A. Nossek†‡
*Huawei Techhnologies Düsseldorf GmbH, German Research Center, 80992 Munich, Germany
†Department of Electrical and Computer Engineering, Technische Universität München, Munich, Germany
‡Department of Teleinformatics Engineering, Federal University of Ceara, Fortaleza, Brazil
Email: {anastasios.kakkavas, wen.dr.xu, jianluo, mario.castaneda}@huawei.com, josef.a.nossek@tum.de

***Abstract*—DFT-s-OFDM/Discrete Fourier Transform (DFT) spread Orthogonal Frequency Division Multiplexing (OFDM) is a waveform adopted in the forth and fifth generation of the mobile communication standards, aiming to combine the merits of Cyclic Prefix (CP) OFDM with a low Peak-to-Average-Power Ratio (PAPR). Due to the growing interest in geometric and probabilistic shaping of the signal constellation, it is important to study the impact of shaping on the power distribution of the corresponding signal. In this work, exact and approximate analytic expressions are derived for the IAPR and PAPR of this waveform, respectively. These expressions can be used for the understanding and comparison of the effects of geometric and probabilistic shaping techniques on the power distribution of the transmitted signal.**

I. Introduction

With the standardization of the next-generation mobile networks (5G) being in progress, an agreement has already been made on the waveforms to be deployed, at least for carrier frequencies up to 40 GHz. Conventional Cyclic Prefix-Orthogonal Frequency Division Multiplexing (CP-OFDM) with the option of receiver-transparent windowing is the waveform of choice for the downlink (DL). For the uplink (UL), two options are agreed, namely CP-OFDM and DFT-s-OFDM (Discrete Fourier Transform spread OFDM, also known as Single Carrier-Frequency Division Multiple Access (SC-FDMA). Despite the advantages it offers, CP-OFDM suffers from high Peak-to-Average Ratio (PAPR). Due to the Power Amplifier (PA) non-linearity, systems have to reduce their transmit power so that the PA operates in its linear region, in order to avoid distortion. A further option to address this problem is to apply PAPR reduction techniques, which result in either increased computational complexity or signal distortion. Mobile users with limited power-budget can benefit from the lower IAPR/Instantaneous to Average Power Ratio and PAPR of DFT-s-OFDM, which leads to potentially higher PA efficiency and allows them to extend their coverage by increasing their transmit power.

Since DFT-s-OFDM is basically a single-carrier waveform, its IAPR/PAPR is largely influenced by the signal constellation used. It is well-known that Gaussian distributed signals are optimal for transmission over Additive White Gaussian Noise (AWGN) channel. The use of conventional uniform Quadrature Amplitude Modulation (QAM) constellations instead results in a performance loss, which is known as the shaping gap and can be as high as 1.53 dB in the high-SNR regime [1], [2]. In the current mobile communications standard, QPSK, 16-QAM, 64-QAM and 256-QAM constellations are used. For the fifth generation, up to 1024-QAM constellations are considered. In addition, the geometric and probabilistic shaping techniques have been proposed as enhanced modulation schemes for 5G [3], [4]. Geometric Shaping (GS) optimizes the distance between the signal constellation points [5], [6], whereas the Probabilistic Shaping (PS) changes the probability distribution of the constellation points to approach Gaussian distribution [7], [8].

Geometric and probabilistic shaping are two promising techniques that aim to close the shaping gap. It is therefore of interest to study their impact on the IAPR/PAPR of the waveform. Approximate expressions for the distribution of the IAPR and PAPR have been provided in [9] and [10], respectively, based on IAPR results of pulse-shaped single-carrier signals, described in [11]. In this work, exact and approximate expressions for the IAPR and PAPR of DFT-s-OFDM using geometrically or probabilistically shaped constellations are provided, with a comparison between the different shaping approaches conducted.

The rest of the paper is organized as follows: The shaping techniques under consideration are reviewed in Section II and the system model is given in Section III. The distribution of the IAPR and PAPR is presented in Section IV. Numerical results and comparisons are provided in Section V, with conclusions drawn in Section VI.

II. Review of Shaping Techniques

In this section we briefly review the shaping techniques, whose IAPR/PAPR is to be evaluated. We focus on constellations with a mean power constraint.

A. Geometric Shaping (GS)

In Geometric Shaping (GS), the conventional uniform QAM constellation in probability and space is replaced by an optimized set of equiprobable signal points, called Non-Uniform Constellation (NUC). The Bit-Interleaved Coded Modulation (BICM) capacity [12] is the most common objective for the optimization of NUCs [13] under a mean power constraint. Other objectives, such as Coded Modulation (CM) capacity [14] and symbol error rate [15] have also been used. NUCs

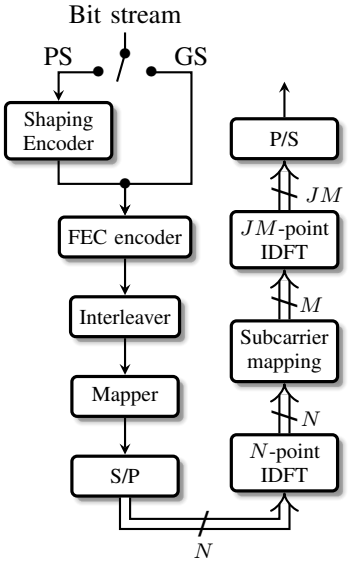

Fig. 1: Block diagram of transmitter processing for DFT-s-OFDM. When PSCM is used, the distribution matcher is added to the processing chain.

can be optimized in one- or two-dimensional space, with the latter resulting in potentially higher performance, at the cost of increased demapping complexity.

B. Probabilistically Shaped Coded Modulation (PSCM)

Although there exist many works on the optimization of the probability distribution of the signal constellation points, we focus on Probabilistically Shaped Coded Modulation (PSCM), or Probabilistic Amplitude Shaping (PAS), proposed in [7]. which does not require iterative demapping and is able to operate close to the capacity of the AWGN channel at any Signal-to-Noise Ratio (SNR). First, a nearly capacity-achieving symbol distribution is computed for a given uniform QAM constellation and the operating SNR. Then, the Constant Composition Distribution Matcher (CCDM), in combination with the Forward Error Correction (FEC) encoder add redundancy to the input bit stream, such that the distribution of the symbols coming out of the mapper becomes nearly capacity achieving. The details for the operation of the CCDM can be found in [16].

III. System Model

We consider a DFT-s-OFDM system with the DFT size N, corresponding to the number of subcarriers assigned to each user and a total number of subcarriers M. For the sake of simplicity we assume M/N is integer. In practical systems, the IAPR/PAPR of the analog signal at the input of the PA is of interest. Such signal results from digital-to-analog conversion, low-pass filtering and up-conversion of the output of the Inverse DFT (IDFT). As in [9], we approximate this band-limited signal by the output of the IDFT oversampled by a factor J. The oversampling operation is implemented here by replacing the M-point IDFT by a JM-point IDFT.

In Fig. 1 the block diagram of the system set-up is shown. The input bit stream is either fed to the distribution matcher for PSCM or directly fed to the systematic FEC encoder when uniform QAM or NUC (GS) is used. Then, the coded bits are mapped to data symbols. The data symbols are points in uniform QAM constellation (uniform QAM and PSCM) or NUC denoted by the set $\mathcal{Q}$, with $|\mathcal{Q}| = Q$. Each of the points $s_q \in \mathcal{Q}, q = 0, \ldots, Q-1$, has an assigned probability p_q. Groups of N symbols $\{s[m]\}_{m=0}^{N-1}$ are spread in the frequency-domain by the N-point DFT. The resulting symbols $\{\tilde{s}[k]\}_{k=0}^{N-1}$ are mapped to the subcarriers assigned to the user. Then the JM-point IDFT is applied to get the oversampled time-domain signal. Here, we assume that the first N subcarriers are used. Then, the n-th output of the IDFT can be expressed as

$$\begin{aligned} x[n] &= \frac{1}{\sqrt{N}} \sum_{k=0}^{N-1} \tilde{s}[k] \mathrm{e}^{\mathrm{j}\,\frac{2\pi}{JM} kn} \\ &= \frac{1}{N} \sum_{k=0}^{N-1} \sum_{m=0}^{N-1} s[m] \mathrm{e}^{-\mathrm{j}\,\frac{2\pi}{N} mk} \mathrm{e}^{\mathrm{j}\,\frac{2\pi}{JM} kn} \\ &= \sum_{m=0}^{N-1} s[m] g[n - mP], \end{aligned} \tag{1}$$

where

$$g[n] = \mathrm{e}^{\mathrm{j}\,\pi\left(1-\frac{1}{N}\right)\frac{n}{P}} \frac{\sin\left(\pi \frac{n}{P}\right)}{N \sin\left(\pi \frac{n}{NP}\right)}, \tag{2}$$

with $P = JM/N$. It is evident from (1), that DFT-s-OFDM is similar to a single-carrier waveform, but instead of a real valued filter, the data symbols are filtered by a complex periodic one. Note that further kind of pulse shaping (e.g. additional filtering of the signal for spectrum confinement) is not considered in this paper, and remains interesting future work.

IV. Instantaneous to Average Power Ratio (IAPR) and Peak to Average Power Ratio (PAPR) Distributions

The IAPR is defined as the ratio of the instantaneous power to the average power of the signal. Assuming that the mean power of the input constellation is equal to 1, it is sufficient to study the distribution of the instantaneous power of $x[n]$. In [11] it was shown that the Cumulative Distribution Function (CDF) of the instantaneous power $F(z;n) = \Pr(|x[n]^2| < z)$ is given by

$$F(z;n) = \sqrt{z} \int_0^\infty J_1(\sqrt{z}R) G(R;n) \mathrm{d}R, \tag{3}$$

where $J_1(\cdot)$ is the first-order Bessel function of the first kind and

$$G(R;n) = \frac{1}{2\pi} \int_0^{2\pi} \Phi_{x_\mathcal{R} x_\mathcal{I}}(R\cos\phi, R\sin\phi; n) \mathrm{d}\phi. \tag{4}$$

$\Phi_{x_\mathcal{R} x_\mathcal{I}}(\omega, \nu; n)$ is the joint characteristic function of $x_\mathcal{R}[n]$ and $x_\mathcal{I}[n]$, which are the real and imaginary part of $x[n]$. Due

to the fact that $|x[n]^2|$ is cyclo-stationary with period P, the Complementary CDF (CCDF) can be simply written as

$$\Gamma(z) = 1 - \frac{1}{P}\sum_{n=0}^{P-1} F(z;n). \tag{5}$$

Unlike [9], [10], in this work we aim to use the exact DFT-s-OFDM filter for the evaluation of the IAPR/PAPR, rather than approximating it with its amplitude. To this end, we define

$$\begin{aligned} f_n &\coloneqq \frac{\sin\left(\pi\frac{n}{P}\right)}{N\sin\left(\pi\frac{n}{NP}\right)} \\ \alpha_n &\coloneqq \pi\left(1-\frac{1}{N}\right)\frac{n}{P} \end{aligned} \tag{6}$$

to obtain

$$\begin{aligned} g[n] &= f_n \mathrm{e}^{\mathrm{j}\,\alpha_n} = f_n\left(\cos(\alpha_n) + \mathrm{j}\sin(\alpha_n)\right) \\ &= g_{\mathcal{R}}[n] + \mathrm{j}\, g_{\mathcal{I}}[n]. \end{aligned} \tag{7}$$

Accordingly, (1) can be rewritten as

$$x[n] = x_{\mathcal{R}}[n] + \mathrm{j}\, x_{\mathcal{I}}[n], \tag{8}$$

where

$$\begin{aligned} x_{\mathcal{R}}[n] &= \sum_{m=0}^{N-1} \boldsymbol{g}_a^{\mathrm{T}}[n-mP]\boldsymbol{s}[m] \\ x_{\mathcal{I}}[n] &= \sum_{m=0}^{N-1} \boldsymbol{g}_b^{\mathrm{T}}[n-mP]\boldsymbol{s}[m] \\ \boldsymbol{s}[m] &= [s_{\mathcal{R}}[m], s_{\mathcal{I}}[m]]^{\mathrm{T}} \\ \boldsymbol{g}_a[n] &= f_n[\cos(\alpha_n), -\sin(\alpha_n)]^{\mathrm{T}} \\ \boldsymbol{g}_b[n] &= f_n[\sin(\alpha_n), \cos(\alpha_n)]^{\mathrm{T}}. \end{aligned} \tag{9}$$

In the following, we derive the expression of this joint characteristic function for the complex filter $g[n]$ and a geometrically or/and probabilistically shaped constellation. First, we express the complex constellation points $s_q, q = 0, \ldots, Q-1$ as real vectors $\boldsymbol{s}_q = R_q[\cos\theta_q, \sin\theta_q]^{\mathrm{T}}$, with the assigned probability p_q. Since $x_{\mathcal{R}}[n]$ and $x_{\mathcal{I}}[n]$ are sums of independent identically distributed random variables, we can write

$$\begin{aligned} \Phi_{x_{\mathcal{R}\mathcal{I}}}(\omega,\nu;n) &= \mathbb{E}_{x_{\mathcal{R}}x_{\mathcal{I}}}\left[\mathrm{e}^{\mathrm{j}(\omega x_{\mathcal{R}}[n]+\nu x_{\mathcal{I}}[n])}\right] \\ &= \prod_{m=0}^{N-1} \mathbb{E}_{\boldsymbol{s}}\left[\mathrm{e}^{\mathrm{j}\left(\omega \boldsymbol{g}_a^{\mathrm{T}}[n-mP]\boldsymbol{s}[m]+\nu\boldsymbol{g}_b^{\mathrm{T}}[n-mP]\boldsymbol{s}[m]\right)}\right] \\ &= \prod_{m=0}^{N-1}\sum_{q=0}^{Q-1} p_q \mathrm{e}^{\mathrm{j}\, f_{n-mP}R_q R\cos(\theta_q+\alpha_{n-mP}-\phi)}, \end{aligned} \tag{10}$$

where $\mathbb{E}_{\boldsymbol{z}}[\cdot]$ is the expectation with respect to $\boldsymbol{z}$. The above equality can be obtaining based on (9) with basic trigonometric identities. Usually for all types of shaped constellations, for every point with probability p_q, amplitude R_q and phase θ_q, there is another point with the same probability and amplitude, but with phase $\theta_q + \pi$. Assuming that for the first $Q/2$ signal points $\theta_q < \pi$, the characteristic function can then be expressed as

$$\begin{aligned} \Phi_{x_{\mathcal{R}\mathcal{I}}}(\omega,\nu;n) = 2\prod_{m=0}^{N-1}\sum_{q=0}^{\frac{Q}{2}-1} p_q \cos\big[f_{n-mP}R_q \\ R\cos(\theta_q+\alpha_{n-mP}-\phi)\big]. \end{aligned} \tag{11}$$

Special care has to be taken for the computation of $F(z;0)$, since it is discontinuous and numerical integration should be avoided. Instead of using (3) directly, it can be computed by

$$F(z;0) = 2\sum_{q=0}^{\frac{Q}{2}-1} p_q H(z - f_0^2 R_q^2), \tag{12}$$

where

$$H(z) = \begin{cases} 1, & z > 0 \\ 1/2, & z = 0 \\ 0, & z < 0. \end{cases} \tag{13}$$

The PAPR is defined as

$$\zeta = \max_{n\in\{0,\ldots,JM-1\}} |x[n]|^2, \tag{14}$$

assuming that $\mathbb{E}\left[|x[n]|^2\right] = 1$, which is true when $\sum_{q=0}^{Q-1} p_q |s_q|^2 = 1$. The steps taken for the computation of the PAPR distribution are identical to those in [10]. The difference lies in the characteristic function, given by (11), which is computed for the complex filter $g[n]$ and general shaped constellations. Relying on the observation that the peak value is most likely to be observed at $n = mP + P/2$ [10], the PAPR CCDF $\tilde{\Gamma}(z)$ can be approximated by

$$\begin{aligned} \tilde{\Gamma}(z) &\approx 1 - \prod_{m=0}^{N-1} \Pr(|x[mP+P/2]|^2 < z) \\ &= 1 - (F(z;P/2))^N \end{aligned} \tag{15}$$

The approximation above is exact if $x[mP + P/2], m = 0, \ldots, N-1$ are jointly Gaussian-distributed.

V. Numerical Results

We now evaluate the derived expressions for the IAPR and PAPR distributions and examine the impact of the various shaping techniques on them. We set the DFT size $N = 64$, the number of subcarriers $M = 256$ and use an oversampling factor $J = 8$. The conventional uniform QAM (Uni-QAM) constellation is used as a benchmark. In our simulations, we also include CP-OFDM with N subcarriers, in order to evaluate the difference in IAPR/PAPR between CP-OFDM and DFT-s-OFDM when shaped constellations are used. In our simulations we compare constellations optimized under a mean power constraint. We compare shaping techniques that target the same spectral efficiency in terms of bits per channel use (bpcu). We set the constellation size $Q = 64$. For Uni-QAM and NUC we use the WiMAX LDPC codes with codeword length 2304 bits and code rate $2/3$. The NUC used is given in [17] for the chosen code rate and is shown

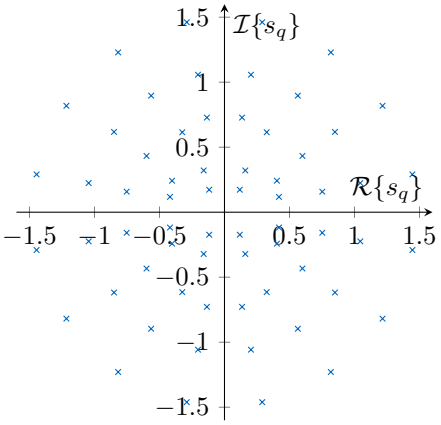

Fig. 2: Geometrically shaped 64-QAM constellation from [17] for code rate $2/3$.

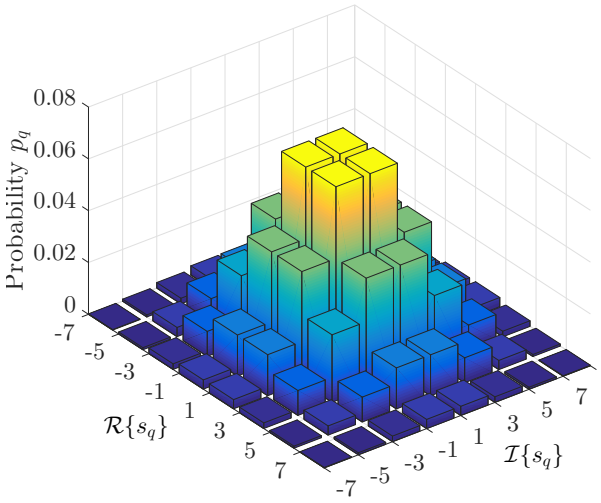

Fig. 3: Optimized probability distribution for a uniform 64-QAM constellation, FEC code rate $5/6$ and a target information rate of 4 bpcu.

in Fig. 2. For PSCM, we use the same channel code, but with rate $5/6$. We set the redundancy introduced by the distribution matcher accordingly to match the information rate of the other schemes, i.e. 4 bpcu. The corresponding optimized probability distribution is shown in Fig. 3.

In Fig. 4 we plot the Frame Error Rate (FER) as a function of the SNR. Here, the SNR is defined as the ratio of the symbol energy E_s to the noise density N_0, for the 3 constellation types (Uni-QAM, NUC and PSCM). Each frame contains one codeword and consists of 6 DFT-s-OFDM blocks. As will be shown, there is a connection between the FER performance (or else the achievable spectral efficiency) and the IAPR/PAPR distribution. As can be observed, PSCM has the best performance, with a 1.04 dB gain at a FER $= 10^{-2}$, while NUC offers a gain of 0.458 dB.

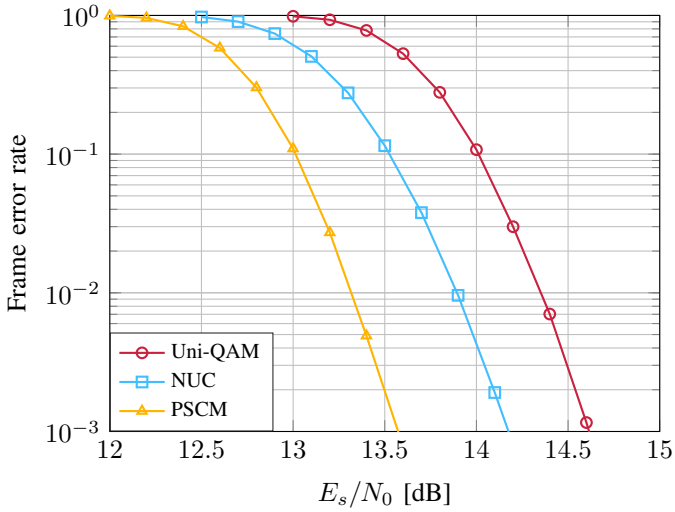

Fig. 4: Frame error rate of DFT-s-OFDM with $N = 64, M = 256$ and $J = 8$ with uniform QAM, NUC from [17] and PSCM for constellation size $S = 64$.

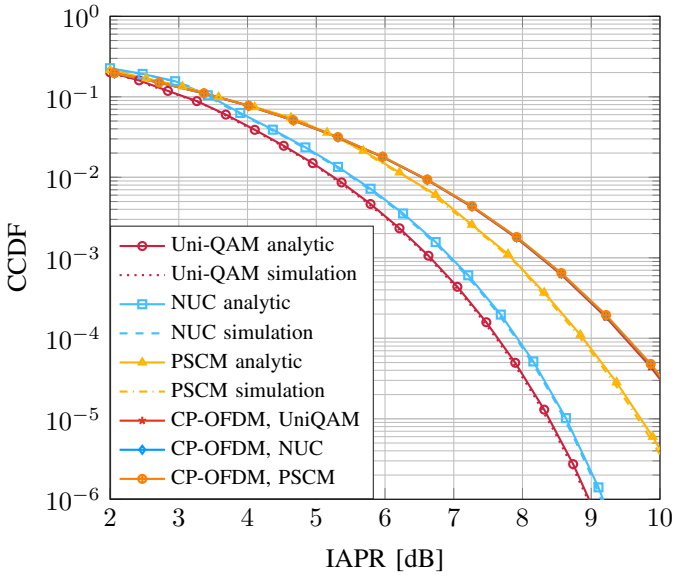

Fig. 5: Analytic and simulated IAPR distribution of DFT-s-OFDM with $N = 64, M = 256$ and $J = 8$ with uniform QAM, NUC from [17] and PSCM for constellation size $Q = 64$.

In Fig. 5 we plot the IAPR CCDF for the setup described above. A perfect match between the analytic and simulated curves can be observed. It is evident that constellation shaping increases the IAPR of the DFT-s-OFDM signal, with PSCM having the largest impact. Also, we can observe that constellation shaping has virtually no impact on the IAPR distribution of the CP-OFDM signal, even for such low number of subcarriers.

In Fig. 6 we plot the PAPR CCDF curve. We can see that for uniform and geometrically shaped constellations the analytic

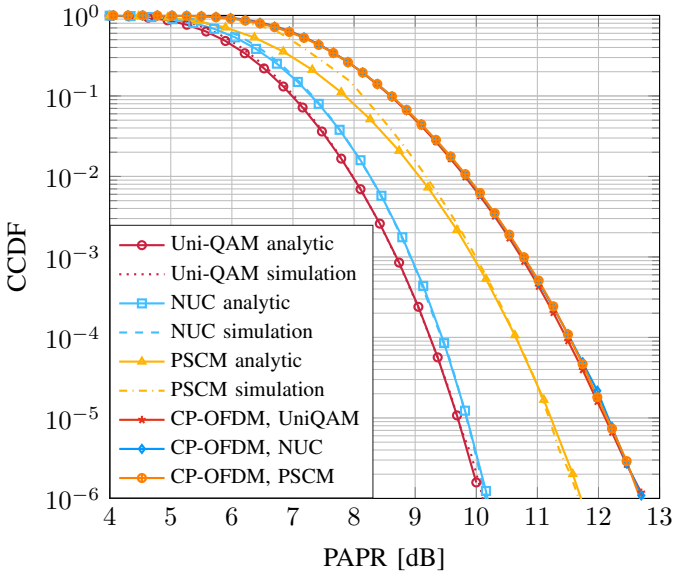

Fig. 6: Analytic and simulated PAPR distribution of DFT-s-OFDM with $N = 64, M = 256$ and $J = 8$ with uniform QAM, NUC from ATSC3.0 and PSCM for constellation size $S = 64$.

and simulated results are very close. For PSCM with high CCDF values the analytic formulas underestimate the PAPR. Nevertheless, for the CCDF region which is usually of interest (10^{-2} to 10^{-4}), the analytic result is in very good agreement with the simulation.

The observations for the impact of shaping on the PAPR of DFT-s-OFDM are identical to those for the IAPR. Same as the IAPR, the PAPR of CP-OFDM is essentially not affected by shaping. Using the uniform QAM constellation as baseline, with a target CCDF value of 10^{-3}, NUC results in a 0.237 dB increase of the PAPR, while PSCM 1.25 dB increase. In order to have a fair comparison among the shaping techniques, we define the net gain as the SNR gain for a FER$= 10^{-2}$ minus the PAPR increase for a CCDF value of 10^{-3}. We use again again using uniform QAM as a benchmark. PSCM and NUC offer a net gain of -0.21 dB and 0.22 dB, respectively.

From the figures above, we can observe that the IAPR/PAPR of the probabilistically shaped DFT-s-OFDM signal comes close to that of CP-OFDM, potentially hindering the application of PSCM on DFT-s-OFDM. Therefore, it is of importance to incorporate peak power constraints, or even constraints using the IAPR/PAPR expressions provided in this paper, for the design of probabilistically shaped constellations.

VI. Conclusion

In this paper, we provided exact expressions for the IAPR and approximate expressions for the PAPR of DFT-s-OFDM with shaped constellations and evaluated them with constellations optimized under a mean power constraint. Our analytic and simulation results show that shaping results in an increase in the IAPR/PAPR, bringing it closer to that of CP-OFDM, which is unaffected by the constellation shaping. PSCM, which is the technique offering the highest spectral efficiency gains, results in the highest IAPR/PAPR increase, too. Therefore, to exploit the potential of probabilistic shaping, peak power constraint has to be taken into account. A possible application of the IAPR/PAPR expressions presented in this work is their inclusion as constraints in the constellation design, by setting a target pair of IAPR/PAPR and corresponding CCDF value.

Acknowledgement

The research leading to these results received funding from the European Commission H2020 program under grant agreements n^{o} 671650 (5G-PPP mmMAGIC project) and n^{o} 671551 (5G PPP 5G-Xhaul project).

References

[1] G. Forney, R. Gallager, G. Lang, F. Longstaff, and S. Qureshi, "Efficient modulation for band-limited channels," *IEEE Journal on Selected Areas in Communications*, vol. 2, no. 5, pp. 632–647, Sep 1984.

[2] L. H. Ozarow and A. D. Wyner, "On the capacity of the Gaussian channel with a finite number of input levels," *IEEE Transactions on Information Theory*, vol. 36, no. 6, pp. 1426–1428, Nov 1990.

[3] R1-1611543, "Performance of non-uniform constellations in nr," Sony, RAN1#87, Reno, USA, Nov. 14–18, 2016.

[4] R1-1701713, "Signal shaping for QAM constellations," Huawei, HiSilicon, RAN1#88, Athens, Greece, Feb. 13–17, 2017.

[5] F.-W. Sun and H. C. A. van Tilborg, "Approaching capacity by equiprobable signaling on the Gaussian channel," *IEEE Transactions on Information Theory*, vol. 39, no. 5, pp. 1714–1716, Sep 1993.

[6] N. S. Loghin, J. Zöllner, B. Mouhouche, D. Ansorregui, J. Kim, and S. I. Park, "Non-uniform constellations for ATSC 3.0," *IEEE Transactions on Broadcasting*, vol. 62, no. 1, pp. 197–203, March 2016.

[7] G. Böcherer, F. Steiner, and P. Schulte, "Bandwidth efficient and rate-matched low-density parity-check coded modulation," *IEEE Transactions on Communications*, vol. 63, no. 12, pp. 4651–4665, Dec 2015.

[8] J. Cho, S. Chandrasekhar, R. Dar, and P. J. Winzer, "Low-complexity shaping for enhanced nonlinearity tolerance," in *ECOC 2016; 42nd European Conference on Optical Communication*, Sept 2016, pp. 1–3.

[9] H. Ochiai, "On instantaneous power distributions of single-carrier FDMA signals," *IEEE Wireless Communications Letters*, vol. 1, no. 2, pp. 73–76, April 2012.

[10] ——, "Peak-to-average power ratio distribution analysis of single-carrier FDMA signals," in *European Wireless 2012; 18th European Wireless Conference 2012*, April 2012, pp. 1–5.

[11] ——, "Exact and approximate distributions of instantaneous power for pulse-shaped single-carrier signals," *IEEE Transactions on Wireless Communications*, vol. 10, no. 2, pp. 682–692, February 2011.

[12] G. Caire, G. Taricco, and E. Biglieri, "Capacity of bit-interleaved channels," *Electronics Letters*, vol. 32, no. 12, pp. 1060–1061, Jun 1996.

[13] J. Zöllner and N. Loghin, "Optimization of high-order non-uniform QAM constellations," in *2013 IEEE International Symposium on Broadband Multimedia Systems and Broadcasting (BMSB)*, June 2013, pp. 1–6.

[14] F. Steiner and G. Böcherer, "Comparison of geometric and probabilistic shaping with application to ATSC 3.0," *CoRR*, vol. abs/1608.00474, 2016. [Online]. Available: http://arxiv.org/abs/1608.00474

[15] G. Foschini, R. Gitlin, and S. Weinstein, "Optimization of two-dimensional signal constellations in the presence of Gaussian noise," *IEEE Transactions on Communications*, vol. 22, no. 1, pp. 28–38, Jan 1974.

[16] P. Schulte and G. Böcherer, "Constant composition distribution matching," *IEEE Transactions on Information Theory*, vol. 62, no. 1, pp. 430–434, Jan 2016.

[17] "ATSC Standard: Physical Layer Protocol (A/322)." [Online]. Available: http://atsc.org/wp-content/uploads/2016/10/A322-2017-Physical-Layer-Protocol.pdf